

**Lifting in equation-free methods for
molecular dynamics simulations of
dense fluids**

*Yves Frederix Giovanni Samaey
Christophe Vandekerckhove Ting Li Erik Nies
Dirk Roose*

Report TW 525, July 2008



Katholieke Universiteit Leuven
Department of Computer Science
Celestijnenlaan 200A – B-3001 Heverlee (Belgium)

Lifting in equation-free methods for molecular dynamics simulations of dense fluids

Yves Frederix Giovanni Samaey
Christophe Vandekerckhove Ting Li Erik Nies
Dirk Roose

Report TW 525, July 2008

Department of Computer Science, K.U.Leuven

Abstract

In the context of multiscale computations, equation-free methods have been developed. In this approach, the evolution of a system is simulated on the macroscopic level while only a microscopic model is explicitly available. To this end, a *coarse time stepper* for the macroscopic variables can be constructed, based on appropriately initialized microscopic simulations. In this paper, we investigate the initialization of the microscopic simulator using the macroscopic variables only (called *lifting* in the equation-free framework) when the microscopic model is a molecular dynamics (MD) description of a mono-atomic dense fluid. We assume a macroscopic model to exist in terms of the lowest order velocity moments of the particle distribution (density, velocity and temperature). The major difficulty is to design a lifting operator that accurately reconstructs the physically correct state of the fluid (i.e., the higher order moments) at a reasonable computational cost. We construct a lifting operator, as well as a *restriction* operator for the reverse mapping. For a simple model problem, we perform a systematic numerical study to assess the time scales on which the lifting errors disappear after reinitialization (*healing*); we also examine the effects on the simulated macroscopic behavior. The results show that, although in some cases accurate initialization of the higher order moments is not crucial, in general a detailed study of the lifting operator is required.

Keywords : multiscale, equation-free computing, initialization, molecular dynamics

Lifting in equation-free methods for molecular dynamics simulations of dense fluids

Yves Frederix[‡] Giovanni Samaey[†] Christophe Vandekerckhove[†] Ting Li[‡]
Erik Nies[‡] Dirk Roose[†]

July 10, 2008

Abstract

Within the context of multiscale computations, equation-free methods have been developed. In this approach, the evolution of a system is simulated on the macroscopic level while only a microscopic model is explicitly available. To this end, a *coarse time stepper* for the macroscopic variables can be constructed, based on appropriately initialized microscopic simulations. In this paper, we investigate the initialization of the microscopic simulator using the macroscopic variables only (called *lifting* in the equation-free framework) when the microscopic model is a molecular dynamics (MD) description of a mono-atomic dense fluid. We assume a macroscopic model to exist in terms of the lowest order velocity moments of the particle distribution (density, velocity and temperature). The major difficulty is to design a lifting operator that accurately reconstructs the physically correct state of the fluid (i.e., the higher order moments) at a reasonable computational cost. We construct a lifting operator, as well as a *restriction* operator for the reverse mapping. For a simple model problem, we perform a systematic numerical study to assess the time scales on which the lifting errors disappear after reinitialization (*healing*); we also examine the effects on the simulated macroscopic behavior. The results show that, although in some cases accurate initialization of the higher order moments is not crucial, in general a detailed study of the lifting operator is required.

1 Introduction

Molecular dynamics (MD) has become an important tool to study phenomena for which continuum models cannot provide sufficient microscopic resolution. Based on statistical physics, one can predict or explain macroscopic or experimentally measurable properties of a system according to the knowledge obtained from the microscopic constituents. While MD has been successfully used for many applications, simulations are necessarily limited to small systems and short time scales, since the computational cost (both with respect to the number of atoms

*yves.frederix@cs.kuleuven.be

[†]Department of Computer Science, K.U.Leuven, Celestijnenlaan 200A, B-3001 Leuven, Belgium

[‡]Polymer Research Division, Department of Chemistry, K.U.Leuven, Celestijnenlaan 200F, B-3001 Leuven, Belgium

and time steps) quickly becomes prohibitive. Many authors have therefore tried to *extend* the time scales of MD simulations; see the recent review [3] and references therein.

Often, however, the time scale limitations can, at least conceptually, be *circumvented* by constructing a coarse model that only takes into account the interactions that are relevant on longer time scales. This problem of time scale separation has been formally addressed in the projection-operator formalism of Zwanzig and Mori [20, 32] by constructing a generalized Langevin equation for the slow dynamics.

In many realistic cases, an analytical derivation of this coarse equation (or its corresponding Fokker-Planck equation) is highly nontrivial. The equation-free framework, as proposed by Kevrekidis and co-workers (see [17] for a review and references), can then be used as a numerical implementation of this projection principle and avoids the explicit construction of the slow manifold and corresponding evolution equation. The main tool is the *coarse time stepper*, which consists of (1) *lifting*, i.e., the creation of appropriate initial conditions for the microscopic model, conditioned upon the coarse state at time t ; (2) *simulation*, using the microscopic model, over the time interval $[t, t + \Delta T]$; and (3) *restriction*, i.e., the extraction of the coarse state at time $t + \Delta T$. Equation-free methods have been used in a wide range of applications and for different types of microscopic models; see, e.g., [7, 19] for examples in which the microscopic model is a kinetic Monte Carlo model consisting of a large ensemble of non-interacting particles.

In this paper, we take the first steps to obtain a rigorous understanding of the properties of the coarse time stepper when MD is used as the microscopic model. To this end, we consider a dense Lennard-Jones fluid contained in a cylinder and subject to a position-dependent external potential. As the macroscopic variables, we consider the lowest order velocity moments of the particle distribution (density, velocity field and temperature). The lifting operator then defines a mapping from these macroscopic variables to an initial position and velocity for each of the particles. The difficulty, however, is to ensure that the generated positions and velocities correctly capture the physical state of the fluid, i.e., the higher order moments of the particle distribution, which are determined by (slaved to) the low order ones. Also, there is the additional complication that particles cannot be positioned too closely to each other; a problem that also appears when dealing with coupled atomistic-continuum simulations, see, e.g., [5, 30].

Several approaches have been proposed to address the lifting problem. The higher order moments could, for instance, be initialized randomly. This introduces a *lifting error*, and one then relies on the separation of time scales to ensure that the higher order moments relax quickly to a functional of the lower order moments (*healing*) [11, 19, 24]. It can be shown that, in some cases, this approach may produce inaccurate results [26, 29]. To initialize the higher order moments correctly, a simulation of the microscopic system should, in principle, be performed with the additional constraint that the lower order moments are kept fixed. This approach was implemented for an MD simulation of a peptide fragment by introducing an external harmonic potential that forces the molecular system towards the desired configuration [13]. How such constraints can be imposed using only a time stepper for the original microscopic system was considered in [9, 10, 27, 28].

Here, we construct a lifting procedure by positioning the atoms on a grid (to ensure a minimal interparticle distance) so that the difference between the resulting and the desired density is minimized; the velocities are initialized using the average velocity and a thermal part

from a space-dependent Maxwell distribution. After lifting, the higher order moments are no longer slaved to the lower order moments, which results in a lifting error. The main contribution of the present paper is a detailed numerical study of the nature of this lifting error, a quantification of the associated healing time, and the effect on the accuracy of the simulated macroscopic behavior. Although MD has been used as the microscopic model in a number of equation-free studies, this paper represents the first detailed study of the properties of the lifting operator in this context. In [13], the MD simulator has been modified to recover the correct higher order moments; in [4] and [21] (in which the related heterogeneous multiscale method is used), the problem was defined in a way that allowed to avoid systematic reinitialization of the MD system. In [4], an ensemble of Lennard-Jones particles was used, of which a fraction is colored. The macroscopic variable was the density of the colored particles, which could be reinitialized without changing the MD ensemble by just relabeling the particles. In [21], changes of the macroscopic variables were imposed on the MD simulation by means of modified boundary conditions.

This paper is organized as follows. In Section 2, the model problem and simulation details for the microscopic system are presented, and we describe the macroscopic behavior of the system. In Section 3, we introduce the equation-free framework and derive suitable restriction and lifting operators for our model problem. Subsequently, we numerically investigate the lifting operator and the evolution of the reinitialized system in Section 4. Finally, conclusions are given in Section 5.

2 Model problem

2.1 Microscopic model

We consider N particles contained in a cylinder with radius R and length L as illustrated in Fig. 1. The x -axis is chosen to coincide with the main axis of the cylinder. For the particle interaction, we use a Lennard-Jones (LJ) potential with cutoff distance $r_c = 2.5\bar{\sigma}$,

$$V_{LJ}(r) = \begin{cases} 4\bar{\epsilon} \left(\left(\frac{\bar{\sigma}}{r} \right)^{12} - \left(\frac{\bar{\sigma}}{r} \right)^6 \right) & r \leq r_c, \\ 0 & r > r_c, \end{cases} \quad (1)$$

with $\bar{\epsilon}$ the potential well depth and $\bar{\sigma}$ the atomic diameter. The cylinder walls are implemented using the repulsive part of a LJ potential, $4\bar{\epsilon}(\bar{\sigma}/r)^{12}$, with the same cutoff distance.

We create an energy barrier by introducing an external potential,

$$\Psi(x) = \begin{cases} A \cos \frac{\pi(x-D)}{\gamma} & |x-D| < \frac{\gamma}{2}, \\ 0 & \text{otherwise,} \end{cases} \quad (2)$$

with A the interface strength, and D and γ parameters that control its location and width.

The particles evolve according to Newton's equations of motion,

$$\begin{aligned} \dot{\mathbf{p}}_i &= \mathbf{v}_i, \\ \dot{\mathbf{v}}_i &= \mathbf{F}_i/m, \quad i = 1, \dots, N, \end{aligned} \quad (3)$$

For our experiments, we choose the Epanechnikov kernel [25] and a fixed bandwidth according to the rule-of-thumb selector proposed by Scott [22].

It is important to note that Eqns. (4), (5) and (6) only define an *estimate* for the macroscopic density, velocity and temperature. While these estimates can be shown to converge for increasing N , gradients in the macroscopic profiles will be smoothed for finite N (as the bandwidth increases for decreasing N). To compute accurate estimates, N can be increased by combining the information of multiple independent runs into a single estimation. The effect on the density estimation is illustrated in Appendix A.

Symmetric case. To illustrate the macroscopic behavior, we initialize the N -particle system with a uniform particle density (using the procedure described below in Section 3.2). The initial velocities are drawn from a Maxwell distribution $P^M(V, T)$ with average velocity $V = 0$ and temperature $T = 1$ (see [12, Appendix 4]), and slightly rescaled so that the total energy becomes exactly $E = 40\,000$. Fig. 2 shows the time evolution of the density $P(x, t)$. For this symmetric macroscopic initial condition, the system exhibits two time scales. On a fast time scale (which corresponds to the time scale of particle movement), a minimum is created in the density profile at the location of the interface (± 200 MD steps). On a slower time scale, we observe the oscillatory relaxation of the density towards a steady state distribution ($\pm 10\,000$ MD steps). Fig. 3 shows the corresponding evolution of the velocity profile $V(x, t)$ towards zero. The temperature is approximately constant after a sharp initial transient, and does not depend significantly on x ; see Fig. 4 (left).

Asymmetric case. In a general case, the external potential will not be a simple symmetric barrier. As a consequence, the steady state particle density will in general not be symmetric either. In this case, a third, slower time scale becomes apparent. Without loss of generality, we can introduce this slowest time scale into our model problem by initializing the reference simulation with an *asymmetric density profile*; the system will then evolve towards a symmetric steady state on a time scale that directly depends on the value of the interface strength A .

The initial condition is determined as follows. We multiply $P(x, t)$ as obtained from the above simulation at $t = 250\,000$ with $S(x) = 1/2H(x) + 3/4$, where $H(x)$ is the Heaviside function [15]. For the resulting density, it then holds that $\int_{-L/2}^0 P(x, 0) dx < \int_0^{L/2} P(x, 0) dx$. To enable us to show this slowest time scale at a reasonable computational cost, we lowered the interface strength to $A = 30$.

Observation of $P(x, t)$ for a number of values of x reveals initial oscillatory behavior, after which evolution takes place on the slowest time scale, see Fig. 5 (left). The corresponding plot for $V(x, t)$ (not shown) reveals similar evolution of the velocity profile towards zero. Fig. 5 (right) shows a number of snapshots of $P(x, t_j)$, which clearly illustrate the evolution towards a symmetric steady state. In Fig. 4 (right), the temperature profile $T(x, t_j)$ is shown for the same values of t_j . We see that a lower density gives rise to a higher local temperature.

Microscopically, individual particle trajectories exhibit chaotic behavior, which results in fluctuations on the macroscopic level. If one performs multiple realizations, it is possible to compute the variance on the macroscopic solution, which gives an indication of the accuracy with which the steady state can be determined. (For our example, the variance on the density is around $\sigma^2 = 10^{-8}$, which corresponds to an error of approximately 1%.)

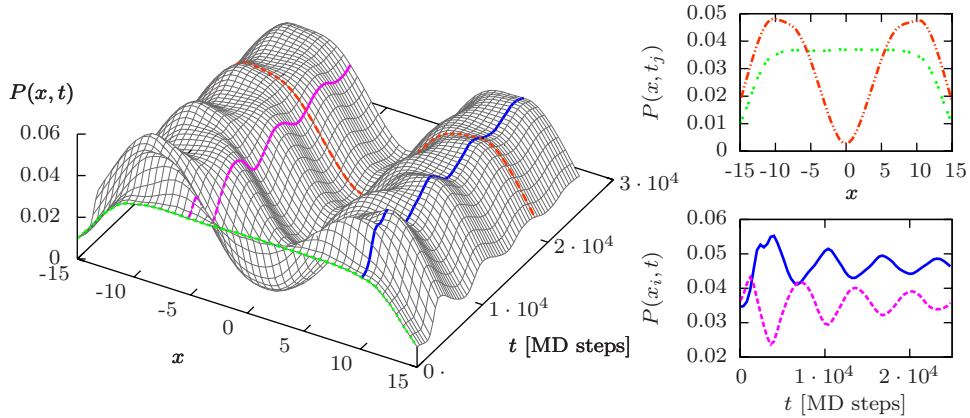


Figure 2: Left: Evolution of the density profile $P(x,t)$ as a function of space and time, starting from a uniform density profile. Top-right: Density $P(x,t_j)$ for $t_j = 0$ (green dash-dash) and $t_j = 18000$ (orange dash-dot-dot). Bottom-right: Evolution in time of $P(x_i,t)$ for $x_i = 10.1$ (blue solid) and $x_i = -5.2$ (magenta dashed).

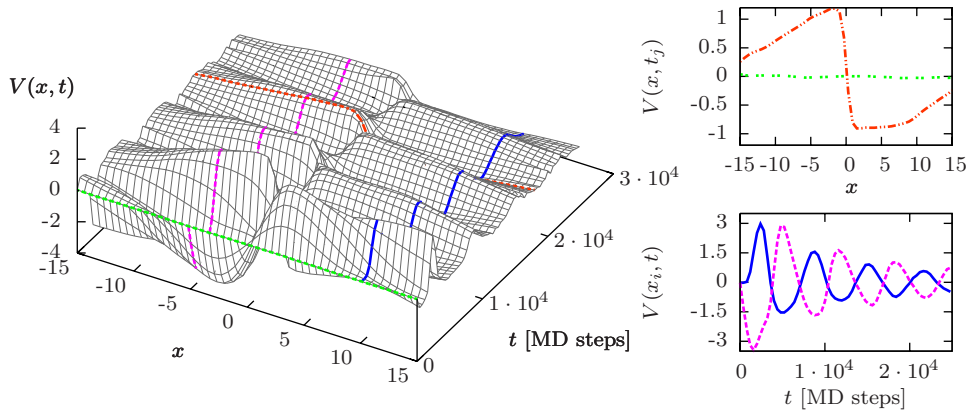


Figure 3: Left: Evolution of the velocity profile $V(x,t)$ as a function of space and time, starting from a uniform velocity profile. Top-right: Velocity $V(x,t_j)$ for $t_j = 0$ (green dash-dash) and $t_j = 18000$ (orange dash-dot-dot). Bottom-right: Evolution in time of $V(x_i,t)$ for $x_i = 10.1$ (blue solid) and $x_i = -5.2$ (magenta dashed).

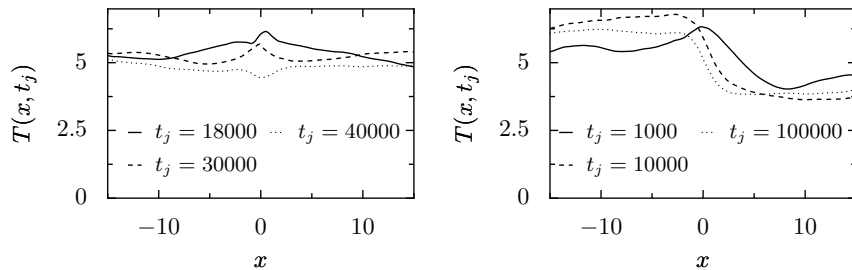


Figure 4: Evolution of temperature profile. Left: $T(x,t_j)$ for symmetric initial conditions. Right: $T(x,t_j)$ for asymmetric initial conditions.

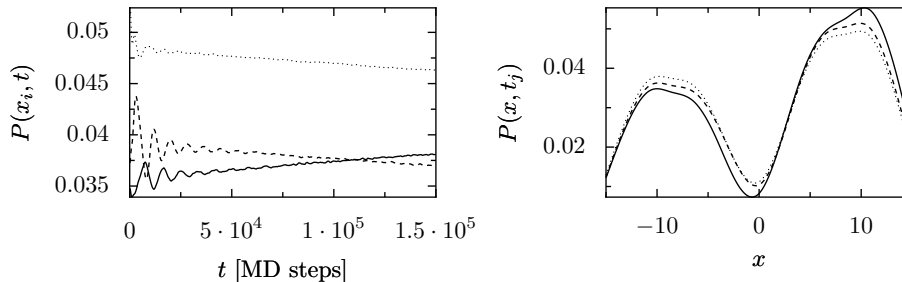


Figure 5: Evolution of $P(x, t)$ for a simulation with asymmetric initial density profile and $A = 30$. Left: $P(x_i, t)$ for $x_i = -8.6$ (solid), 4.3 (dashed) and 6.4 (dotted). Right: $P(x, t_j)$ for $t_j = 1000$ (solid), 10000 (dashed) and 100000 (dotted).

3 Equation-free methods

Within the equation-free framework [17], the main task is to build a coarse time stepper (CTS) for (a spatial discretization of) the macroscopic variables $\mathbf{U}(x, t) = (P(x, t), V(x, t), T(x, t))$, using only simulations with the microscopic MD model. To this end, we need to introduce a lifting operator μ and the corresponding restriction operator \mathcal{M} . The lifting operator,

$$\mu : \mathbf{U}(x, t) \mapsto \mathbf{u}(x, t) = \{\mathbf{p}_i, \mathbf{v}_i\}, i = 1, \dots, N, \quad (7)$$

creates initial positions and velocities, given the density, velocity and temperature. The restriction operator,

$$\mathcal{M} : \mathbf{u}(x, t) \mapsto \mathbf{U}(x, t), \quad (8)$$

does the opposite. Ideally, $\mathcal{M}\mu \cong I$, i.e., restriction directly after lifting should have negligible effect. As we will show later, we are not able to ensure a strict equality. The lifting procedure is typically the more difficult operation, as it constitutes a one-to-many mapping.

Once these operators are determined, a CTS can be defined as

$$\mathbf{U}^{k+1} = \Phi_{\Delta T}(\mathbf{U}^k) = \mathcal{M}(\phi_{\Delta T}(\mu(\mathbf{U}^k))), \quad (9)$$

with $\phi_{\Delta T}(\mathbf{u})$ the MD simulator that evolves the microscopic system over time ΔT . To reduce the variance on the macroscopic level, one can perform multiple replica simulations and average the result. The CTS can directly be plugged into existing numerical tools to compute or analyze the macroscopic behavior. For instance, it can be used in a *coarse projective integration* scheme [17], to numerically accelerate the macroscopic dynamics. Other applications include macroscopic steady state calculation or bifurcation analysis.

In Section 3.1 we will define a restriction operator for our model problem. Section 3.2 presents the lifting operator.

3.1 Restriction

In Section 2.2, we defined the macroscopic state $\mathbf{U}(x, t)$ using KDE as in Eqs. (4)–(6). Since this representation is still N -dimensional, we approximate $P(x, t)$, $V(x, t)$ and $T(x, t)$ with an interpolating cubic B-spline with equidistant points. The required number of interpolation

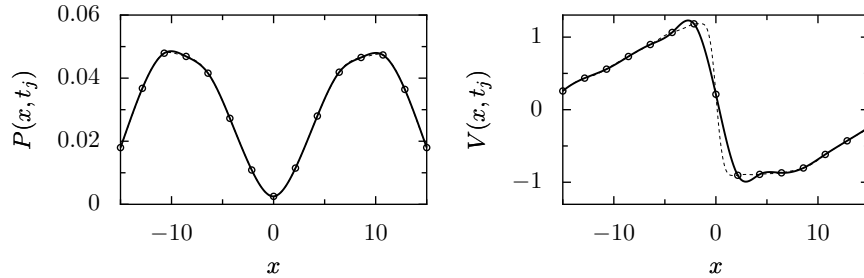


Figure 6: Kernel density estimation (dashed) and interpolating spline approximation (solid) for the density (left) and velocity profile (right) for the symmetric case in Section 2.2 at $t_j = 18000$. The interpolation points are indicated by circles.

points is determined by the smoothness of the solution and the desired resolution. Fig. 6 shows the full KDE and the spline approximation for both $P(x, t_j)$ (left) and $V(x, t_j)$ (right) at $t_j = 18000$ for the symmetric case described in Section 2.2 (see also Figs. 2 and 3). For $T(x, t_j)$, the results are similar (not shown). We observe that, for our model problem and a non-steady state configuration, 15 interpolation points are sufficient, resulting in a reduction from 30 000 to 45 variables.

3.2 Lifting

Designing a good lifting operator, i.e., generating initial conditions for the particle positions \mathbf{p}_i and velocities \mathbf{v}_i from only $P(x, t)$, $V(x, t)$ and $T(x, t)$, is non-trivial, especially for dense fluids. We perform lifting in two consecutive steps:

1. Choose adequate positions \mathbf{p}_i based on $P(x, t)$.
2. Given the values of \mathbf{p}_i , initialize the velocities \mathbf{v}_i based on $V(x, t)$ and $T(x, t)$.

Positions. To ensure that the particles are placed not too close to each other, they are positioned on a regular face-centered cubic (fcc) grid. For this type of packing, the minimal distance between the grid positions d_g and the distance between the grid planes Δx are related by $d_g = \sqrt{3/2}\Delta x$. As we are dealing with a Lennard-Jones fluid, we choose $d_g \geq \bar{\sigma}$. To avoid artifacts near the left and right cylinder wall, we place the grid at a distance d_g from the cylinder endings and choose d_g the smallest value larger than or equal to $\bar{\sigma}$ so that

$$n\Delta x = n\sqrt{2/3}d_g = L - 2d_g, n \in \mathbb{N}, \quad (10)$$

with n the number of planes.

Only grid positions that lie inside the cylinder are used. For all experiments reported in this article, we use $n = 33$ grid planes.

Let α_i denote the number of particles in the plane located at $x = X_i$. We rewrite Eq. (4) as

$$P(x, t) = \frac{1}{Nh} \sum_{i=1}^n \alpha_i K\left(\frac{x - p_{x,i}(t)}{h}\right), \quad \text{with } \sum_i \alpha_i = N. \quad (11)$$

We now want to determine the integers α_i that minimize the difference between the reference density $P(x, t)$ and the restriction of the lifted configuration $\bar{P}(x, t)$. When lifting is performed at $t = \tau$, this results in the optimization problem

$$\min \int_{-L/2}^{L/2} |P(x, \tau) - \bar{P}(x, \tau)| dx, \quad \text{s.t.} \sum_{i=1}^n \alpha_i = N. \quad (12)$$

We discretize the integral in Eq. (12) via the midpoint rule and rescale to obtain

$$\min \sum_{j=1}^q |P(x_j, \tau) - \bar{P}(x_j, \tau)|, \quad \text{s.t.} \sum_{i=1}^n \alpha_i = N, \quad (13)$$

with $x_j \in [-L/2, L/2]$ a set of q integration points. Using a fixed bandwidth h , Eq. (13) can be reformulated as a linear programming (LP) problem [2, Section 5].

Note that Eq. (13) is an *integer* optimization problem in α_i , which is hard to solve. To limit computational cost, we solve the *non-integer* problem and round the result afterwards without breaking the constraints [31], i.e., the rounded values $\bar{\alpha}_i$ fulfill $\sum_i \alpha_i = N = \sum_i \bar{\alpha}_i$. Note that the kernel bandwidth is unknown beforehand; it is automatically determined during the KDE restriction. Therefore, the LP problem is solved repeatedly in an iterative process, using the optimal h for the current solution as input for a new optimization step. It was verified that this process indeed quickly converges to a fixed h .

The above procedure only defines the number of particles in every grid plane. We choose the remaining y and z coordinates randomly from the available grid positions within the corresponding plane using a uniform probability distribution, which is in agreement with observations from simulation.

Velocities. In general, reinitialization of the particle positions will change the potential energy after reinitialization $\bar{E}_p \neq E_p$. Therefore, during the reinitialization of the velocities, the kinetic energy E_k (or correspondingly, the temperature) needs to be rescaled to keep the total energy E constant. This is accomplished as follows. The particle velocities \mathbf{v}_i are initialized from the macroscopic velocity $V(x, \tau)$ and temperature $T(x, \tau)$ using a local Maxwell distribution,

$$\mathbf{v}_i = \begin{bmatrix} V(p_{i,x}, \tau) \\ 0 \\ 0 \end{bmatrix} + C \cdot \sqrt{T(p_{i,x}, \tau)} \cdot P^M(0, 1), \quad (14)$$

in which the normalization constant C is chosen to conserve the total energy. (The assumption that the thermal part of the velocity satisfies a Maxwell distribution was verified using a long reference simulation.) The normalization results in a lifting error, of which the effect will be studied in Section 4.1. The full lifting procedure is summarized in Algorithm 1.

To assess the quality of the above procedure, we compare the original macroscopic profile and the profile calculated from the lifted configuration. First, we define $\bar{V} = \mathcal{M}\mu V$ similarly to \bar{P} . The results for the asymmetric case of Section 2.2 at $\tau = 75000$ are given in Fig. 7 for the particle density (left), velocity (right) and temperature (bottom). We observe good agreement between the original and reinitialized system, indicating that the normalization constant $C \approx 1$.

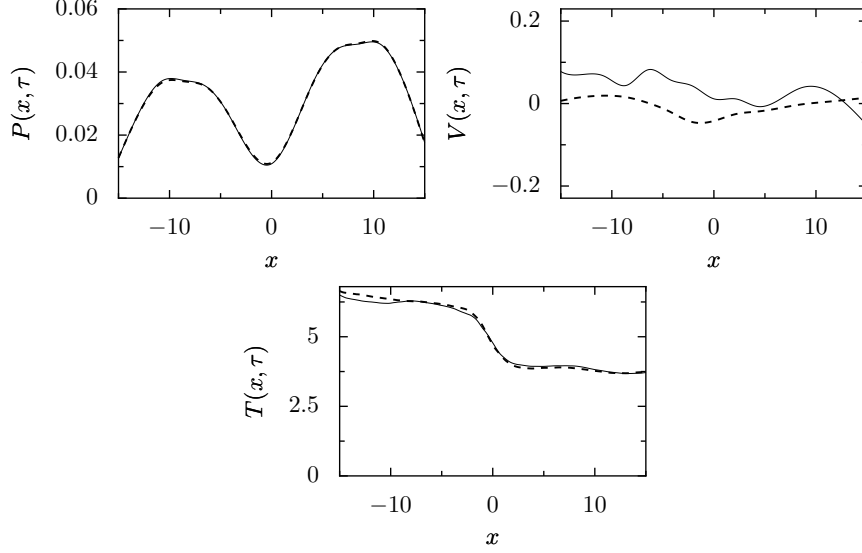


Figure 7: Comparison of the reference profile and the lifted profile for the asymmetric case of Section 2.2 at $\tau = 75\,000$. Left: Density profile $P(x, \tau)$ (dashed) versus $\bar{P}(x, \tau)$ (solid). Right: Velocity profile $V(x, \tau)$ (dashed) versus $\bar{V}(x, \tau)$ (solid). Bottom: Temperature profile $T(x, \tau)$ (dashed) versus $\bar{T}(x, \tau)$ (solid).

Algorithm: Lifting procedure.

Solve Eq. (13) as a non-integer LP problem for α_i .

Round α_i so that $N = \sum_i \alpha_i = \sum_i \bar{\alpha}_i$.

Randomly choose $\bar{\alpha}_i$ grid positions inside each plane i .

Determine $\mathbf{V}_{\text{avg},j} = [V(p_{j,x}), 0, 0], \forall j$.

Determine $T_j = T(p_{j,x}), \forall j$.

Draw velocities \mathbf{V}_{th} from $P^M(0, 1)$.

Calculate C so that $\bar{E}_p(\mathbf{p}_j) + E_k(\mathbf{V}_{\text{avg},j}, \mathbf{V}_{\text{th},j}, C) = E$.

Assign $\mathbf{v}_j = \mathbf{V}_{\text{avg},j} + C \cdot \sqrt{T_j} \cdot \mathbf{V}_{\text{th},j}, \forall j$.

Algorithm 1: Full lifting procedure

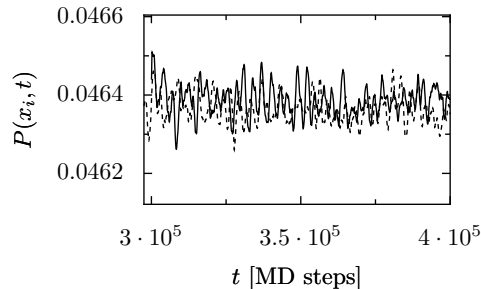


Figure 8: Effect of reinitialization on the density profile $P(x_i, t)$ for $x_i = -8.6$. Comparison of a reference simulation initialized from a uniform density profile (dashed) and a simulation that was reinitialized at $\tau = 300\,000$ (solid), both averaged over 50 replica simulations.

Note that $\bar{\mathbf{U}} = \mathcal{M}\mu\mathbf{U} \approx \mathbf{U}$. For the density, this approximation holds quite well. The slightly larger discrepancy for $\bar{V}(x, \tau)$ can be explained by noting that a KDE approximation of the evaluation of $V(x, t)$ at N points, followed by recomputation of $\bar{V}(x, t)$ as the KDE of this new set of N samples, generally does not exactly reconstruct the original $V(x, t)$. The error in the temperature directly depends on C , and relaxes on a fast time scale towards the correct value (see below).

4 Numerical study of the effect of reinitialization

We now study the behavior of the model problem after reinitialization using Algorithm 1. The procedure is validated via comparison with a long microscopic reference simulation, which is obtained as the average of 50 replica simulations with total energy $E = 40\,000$, as in Section 2.2. At a given time $t = \tau$, we reinitialize the 50 replica simulations and compare the evolution of the averaged macroscopic variables after reinitialization $\bar{\mathbf{U}}(t)$ with the reference trajectory $\mathbf{U}^*(t)$.

4.1 Reinitialization from steady state

We start from a uniform initial density profile (cf. Section 2.2) and, as a first test, reinitialize at $t = \tau = 300\,000$ using Algorithm 1. At this value of t , the macroscopic variables have reached a steady state, which should be preserved under reinitialization. As was seen in Fig. 4, the temperature can in this case be approximated by a constant, so that we can combine $C\sqrt{T_i}$ (see (14)) into a single normalization constant \bar{C} . Fig. 8 shows $P^*(x_i, t)$ and $\bar{P}(x_i, t)$ for $x_i = -8.6$; the steady state of the density is clearly preserved. Similar results are obtained for other values of x_i . Next, we illustrate the effect of reinitialization on the velocity profile; see Fig. 9. Immediately after the restart, the velocity profile deviates from the profile of the reference run. This kick disappears after approximately 5000 MD steps.

We also examine the effects on the energy. While the total energy E is kept constant during reinitialization, the lifting perturbs the balance between potential and kinetic energy. If the grid distance d_g is chosen according to Eq. (10), the initial potential energy E_p is lower than before reinitialization, which results in an increased kinetic energy (and temperature). In Fig. 10, we compare the evolution of the potential energy in the restarted simulations with

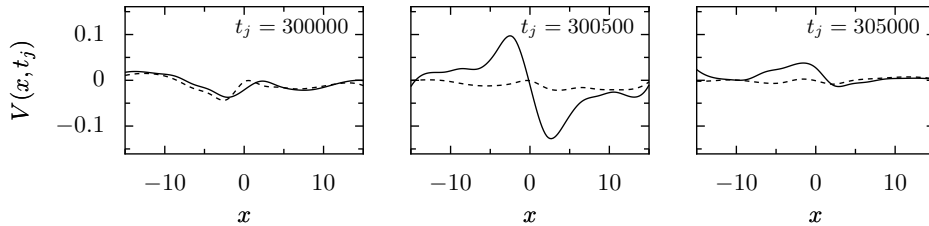


Figure 9: Effect of reinitialization on the velocity profile $V(x, t_j)$. Comparison of a reference simulation initialized from a uniform density profile (dashed) and a simulation that was reinitialized at $\tau = 300\,000$ (solid), both averaged over 50 replica simulations. The kick disappears after 5000 MD steps.

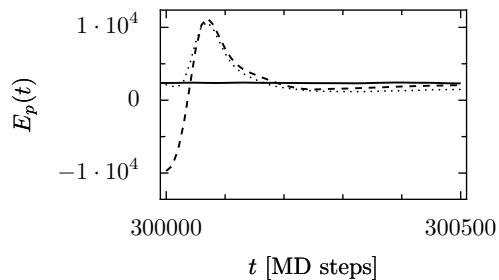


Figure 10: Comparison of $E_p(t)$ from the reference simulation (solid) and a simulation that was reinitialized at $\tau = 300\,000$. Shown are $\overline{E_p}(t)$ for an isotropic grid according to Eq. (10) (dashed) and for a correctly initialized E_p (dotted). A kick over 200 MD steps in the potential energy after reinitialization is observed in both cases.

the reference simulation. We see that, indeed, $\overline{E_p} < E_p$ at $t = \tau$; however, during the first 200 MD steps, $\overline{E_p}$ exhibits an upward kick after which it relaxes towards the correct energy. One could remedy the imbalance between potential and kinetic energy by including E_p as an extra macroscopic variable; to ensure a correct initialization $\overline{E_p} \approx E_p$, we can then adjust the grid distance d_g , which determines the potential energy and consequently the kinetic energy. This requires an iterative procedure to minimize the difference between the required and obtained potential energy. The results of an experiment, in which we have ensured a correct balance between potential and kinetic energy, are shown in Fig. 10. We see that, although $|E_p(t) - \overline{E_p}(t)|$ is small at $t = \tau$, we observe a similar upward kick as before. Moreover, the evolution of the velocity profile (not shown) exhibits the same kick as was observed in Fig. 9. Hence, we conclude that a correct initialization of E_p (and, as a result, a correct initialization of the temperature) does not have a significant impact on the results, and the computational effort cannot be justified. To gain insight in the microscopic structure of the system, we now consider the radial distribution function $g(r)$ [1], which describes the density of a substance as a function of the distance from a given particle. From the shape of the curve, conclusions related to, e.g., the phase of the substance can be drawn. Fig. 11 compares $g^*(r, t)$ of the reference run with $\overline{g}(r, t)$ of the reinitialized simulation. We illustrate the time evolution of $g(r, t)$ immediately after the reinitialization via a series of snapshots at $t_j = 300\,010$, $300\,100$ and $300\,400$. The initially high, sharply peaked shape reflects the fact that the particles are located on a regular grid and is typical for a solid. Over 500 MD steps, the particle positions relax towards the correct fluid-like configuration; see Fig. 11 (right).

The analysis of the reinitialization effects in the steady state revealed two phenomena. First,

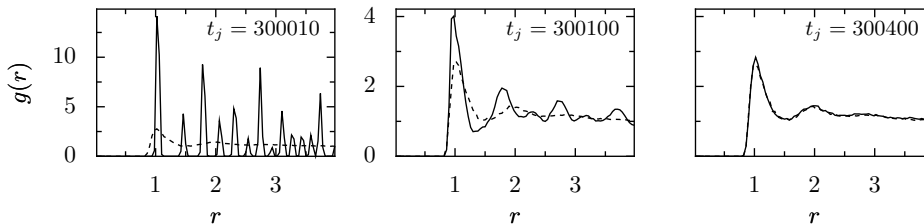


Figure 11: Evolution of the radial distribution functions $\bar{g}(r,t)$ (solid) and $g^*(r,t)$ (dashed) when reinitializing at $\tau = 300\,000$. Both simulations are averaged over 50 replica simulations. Given are snapshots at $t_j = 300\,010$, $300\,100$ and $300\,400$.

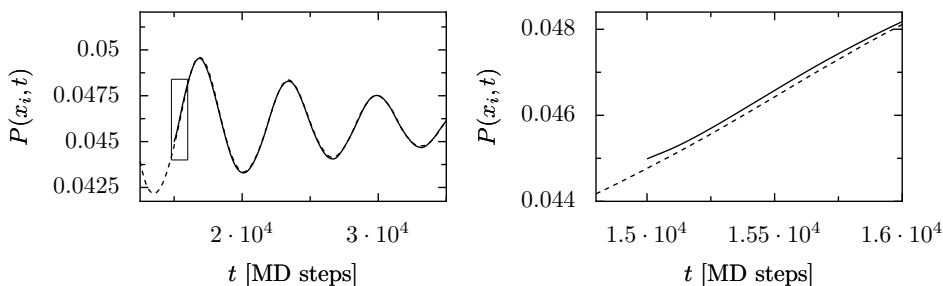


Figure 12: Effect of reinitialization on the density profile $P(x_i, t)$ for $x_i = -10.7$. Left: Comparison of the reference simulation initialized from a uniform density profile (dashed) and a simulation that was reinitialized at $t = \tau = 15\,000$ (solid), both averaged over 50 replicas. Left: $P(x_i, t)$. The lines are indistinguishable. Right: Zoom around $\tau = 15\,000$. The small discontinuity in the trajectory indicates the small lifting error at the restart point.

the time evolution of the radial distribution function and the potential energy suggests a healing time of approximately 500 MD steps, during which the microscopic system relaxes (“melts”) from its artificial state to regain its correct fluid-like configuration; this healing time can be considered as the time it takes for the system to return to a microscopically realistic state. However, we also observed significant changes to the macroscopic variables on a time scale that is an order of magnitude larger than the healing time; this is similar to what was reported in [26, 29]. As a result, in an equation-free context, it might be required to use larger ΔT in the CTS to allow for the macroscopic variables to relax as well.

4.2 Symmetric initial state

As a next step, we investigate the transient behavior when starting from a symmetric initial condition. To this end, we repeat the previous experiment, but we now reinitialize at $t = \tau = 15\,000$. A comparison of $P^*(x_i, t)$ and $\bar{P}(x_i, t)$ for $x_i = -10.7$ is given in Fig. 12. We observe good reconstruction of the reference trajectory by the reinitialized run. Similar results are obtained for the density $P(x_i, t)$ for other values of x_i , as well as for the velocity profile.

Next, we investigate the long term behavior of a coarse time stepper $\Phi_{\Delta T}(\mathbf{U}(t))$ (9), as a function of the coarse time step ΔT (the time between successive reinitializations). We compare $P^*(x_i, t)$ to $\bar{P}(x_i, t)$ for $x_i = -10.7$ and increasing values of ΔT ; see Fig. 13. For $\Delta T = 500$ (left), i.e., a run long enough to ensure microscopic healing of the system,

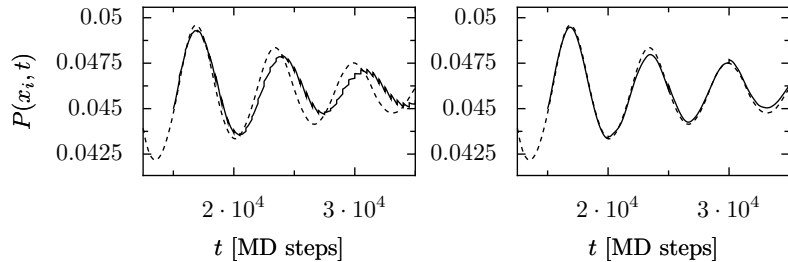


Figure 13: Comparison of $P(x_i, t)$ with $x_i = -10.7$ for a reference simulation (dashed) and a CTS (solid) for different values of ΔT . Left: $\Delta T = 500$. Right: $\Delta T = 5000$.

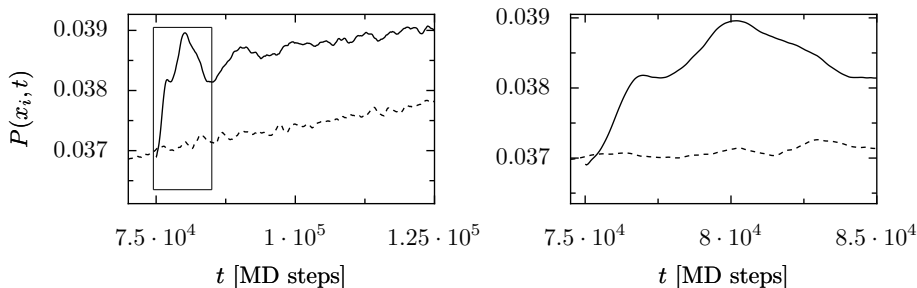


Figure 14: Left: Density $P^*(x_i, t)$ (dashed) and a single reinitialization $\bar{P}(x_i, t)$ (solid) for $x_i = -8.6$ for the asymmetric case, averaged over 50 realizations. Right: Zoom directly after reinitialization.

we see a large deviation from the reference simulation. We find that larger values of ΔT (e.g., $\Delta T \geq 5000$) are required to obtain a sufficiently accurate macroscopic trajectory (right). This can be explained by the fact that, during the healing, the macroscopic velocity changes significantly and only recovers on longer time scales.

It is important to point out that the required value $\Delta T \geq 5000$ is almost as large as half a period of the macroscopic oscillation. Hence, in the context of equation-free acceleration techniques, coarse projective integration cannot provide a large speedup of the macroscopic dynamics.

4.3 Asymmetric initial state

As a final step, we investigate the effects of reinitialization when the density profile is asymmetric. The reference solution is obtained as in Section 2.2. We reinitialize the system using the coarse description at $t = \tau = 75\,000$ (after the initial oscillatory behavior) and consider $\bar{P}(x_i, t)$.

To illustrate the importance of the local temperature, we first perform an experiment where, as before, we use a uniform temperature. The results for the density are shown in Fig. 14. We start from the correct macroscopic state at $\tau = 75\,000$, followed by oscillatory behavior over 25 000 MD steps, after which the *slow* dynamics strongly differ from the reference simulation. In other words, the macroscopic variables change significantly during the healing phase, which has an irreparable effect, also on the density, and a different macroscopic trajectory is followed once the system has healed. Fig. 15 shows the evolution of the density and velocity profile

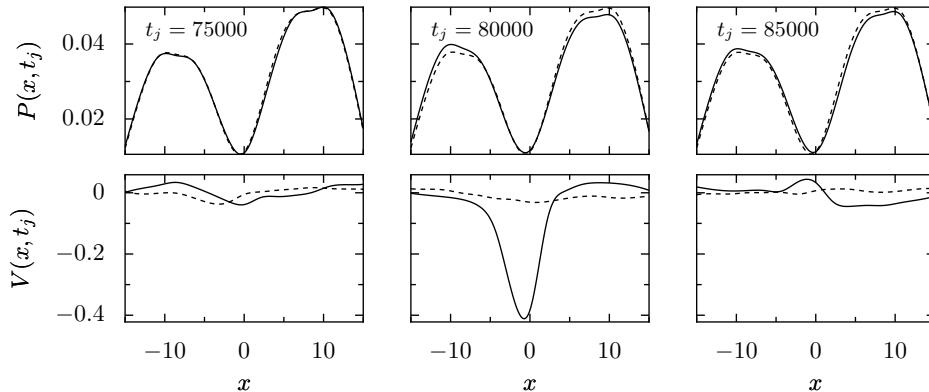


Figure 15: Snapshots at $t = 75\,000$, $80\,000$ and $85\,000$ for the macroscopic density (first row) and velocity (second row) for a reinitialization at $t = \tau = 75\,000$ (solid) from a reference run with asymmetric initial state (dashed), both averaged over 50 realizations. A negative velocity kick over 10 000 MD steps is observed, which manifests itself on the level of the density profile already over shorter time scales.

of the restarted and reference simulations. Immediately after the restart, we observe a kick towards negative velocity (second row). After 5000 MD steps, this has resulted in a significant change in the density profile (first row).

To show that this behaviour cannot be attributed to the positioning of particles on a grid, we repeat the same experiment; however, we now retain *exact* particle positions from the reference simulation and only apply the lifting procedure to the velocities (with uniform temperature). The resulting evolution of density and velocity profiles is nearly identical.

As was shown in Section 2.2, the temperature profile is not uniform in x when the density is asymmetric. We therefore perform a second experiment, in which we use Eq. (14) for the initialization of the velocities taking into account the complete temperature profile. First, we again only reinitialize the particle velocities (using the exact microscopic particle positions from the reference simulation). Fig. 16 (left) shows that the reinitialized trajectory is almost identical to the reference simulation, which suggests that when the temperature profile is not uniform, the reconstruction of the correct local variance of the particle velocities is crucial for correct dynamics.

However, if we perform a complete lifting of positions *and* velocities (using the local temperature), and again compare the evolution of the density with the reference simulation, we again see a deviation, albeit smaller than when using a spatially uniform temperature; see Fig. 16 (right). This experiment indicates that, although it is *necessary* to take into account the temperature profile as a macroscopic variable during the lifting, it is not *sufficient*. Apparently, the repositioning of the particles on a grid has a subtle effect on higher order correlations in the system that are important, but not reconstructed by the lifting operation. This effect only becomes apparent in the asymmetric case. This behaviour is analogous to the observations that were made in [26, 29] for lattice Boltzmann models. To avoid the associated errors, the lifting step should include a constrained simulation phase, during which the microscopic system evolves subject to the constraint that the macroscopic variables are kept fixed, similarly to the constrained runs algorithm that was proposed and analyzed in [9, 10, 27, 28].

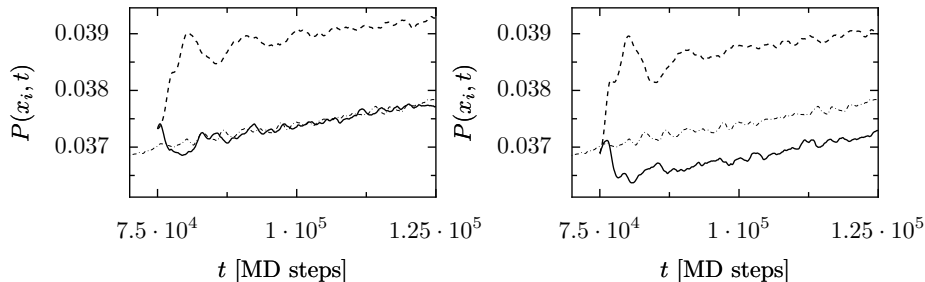


Figure 16: Evolution of $P^*(x_i, t)$ (dash-dot) and a single reinitialization $\bar{P}(x_i, t)$ for $x_i = -8.6$ and $\tau = 75\,000$ for the asymmetric case. Left: Reinitialization using exact positions with uniform (dashed) and complete (solid) temperature profile. Right: Reinitialization using lifted positions with uniform (dashed) and complete temperature profile (solid).

5 Discussion and conclusions

We have constructed lifting and restriction operators to perform the mapping from macroscopic variables to a molecular dynamics description of a dense mono-atomic fluid, and vice versa. The macroscopic state was considered to be given by the lower order moments of the particle distribution (density, velocity and temperature); these were estimated from the particle positions and velocities using spline interpolation of a kernel density estimation. For the lifting operator, a position and velocity was assigned to each particle, according to the macroscopic state. To ensure that a meaningful initial position could be found for every particle, we placed the particles on a grid. The positions on the grid were chosen to minimize the difference between the desired density and the restriction of the lifted density. The velocities were assigned from the macroscopic velocity field, to which a thermal component was added from a Maxwell distribution corresponding to the local temperature. The velocities were rescaled to conserve total energy.

The lifting operator inevitably leads to errors in the higher order moments, of which we investigated the effects in full detail. We performed a systematic numerical study for a model problem, describing an ensemble of Lennard-Jones particles in a cylinder with a potential barrier. We assessed the time scales on which the lifting errors disappear after reinitialization (*healing*); we also examined the effects on the simulated macroscopic behavior.

The results show that, although in some cases accurate initialization of the higher order moments is not crucial, in general a detailed study of the lifting operator is necessary to be able to perform equation-free computations. For the model problem, in particular, we observed that it was possible to neglect the higher order moments when the initial condition was symmetric, provided the coarse time step was chosen large enough. To determine the size of the coarse time step, it is not sufficient to consider healing of the microscopic state of the system, since reinitialization can also have an effect on the evolution of the macroscopic state that only disappears on longer time scales; this is similar to what was observed for lattice Boltzmann models in [26, 29]. For an asymmetric initial condition, however, we showed that an irreparable error is introduced in the macroscopic evolution, even though all macroscopic variables are initialized correctly. We demonstrated numerically that higher order correlations between the particle positions are destroyed, due to the fact that particles are positioned on a grid. We remark that we do not observe an improvement when using alternative (more

irregular) point sets that guarantee a minimal interparticle distance, such as Poisson sphere distributions [18]. Instead, a constrained simulation is needed for accurate lifting, similar to the constrained runs algorithm [9, 10, 27, 28]. How this can be done efficiently when using MD as the microscopic model, is the topic of current research.

As a final remark, we want to emphasize that the aim of using a coarse time stepper is to obtain a macroscopic solution (steady states, transients) with significantly less computational effort than a full microscopic simulation. The computational gain depends on the relation between two (essentially independent) factors: (1) the computational effort that is required during the lifting and the length of the coarse time step to assure sufficient healing; and (2) the time scales of the macroscopic evolution. While the model problem considered in this paper allows to clearly identify all important aspects of the lifting operator, quantitative statements will depend on the specific application.

Acknowledgments

The authors would like to thank Bill Gear, Yannis Kevrekidis and Sebastian Reich for useful discussions.

This paper presents research results of the Belgian Network DYSCO (Dynamical Systems, Control, and Optimization), funded by the Interuniversity Attraction Poles Programme, initiated by the Belgian State, Science Policy Office. The scientific responsibility rests with its authors. GS is a Postdoctoral Fellow of the Research Foundation - Flanders (FWO).

References

- [1] M. P. Allen and D. J. Tildesley. *Computer simulation of liquids*. Clarendon Press, New York, NY, USA, 1989.
- [2] A. Charnes, W. W. Cooper, and R. O. Ferguson. Optimal estimation of executive compensation by linear programming. *Management Science*, 1(2):138–151, 1955.
- [3] A. Chatterjee and D. Vlachos. An overview of spatial microscopic and accelerated kinetic Monte Carlo methods. *Journal of Computer-Aided Materials Design*, 14(2):253–308, 2007. 10.1007/s10820-006-9042-9.
- [4] L. Chen, P. G. Debenedetti, C. W. Gear, and I. G. Kevrekidis. From molecular dynamics to coarse self-similar solutions: a simple example using equation-free computation. *Journal of Non-Newtonian Fluid Mechanics*, 120(1-3):215–223, 2004.
- [5] R. Delgado-Buscalioni and P. V. Coveney. USHER: An algorithm for particle insertion in dense fluids. *Journal of Chemical Physics*, 119(2):978–987, 2003.
- [6] J. Eapen, J. Li, and S. Yip. Statistical field estimators for multiscale simulations. *Physical Review E*, 72(5):056712–1–056712–16, 2005.
- [7] R. Erban, I. G. Kevrekidis, and H. G. Othmer. An equation-free computational approach for extracting population-level behavior from individual-based models of biological dispersal. *Physica D: Nonlinear Phenomena*, 215(1):1–24, 2006.

- [8] D. Frenkel and B. Smit. *Understanding Molecular Simulation: From Algorithms to Applications*. Academic Press, Inc., Orlando, FL, USA, 1996.
- [9] C. W. Gear, T. J. Kaper, I. G. Kevrekidis, and A. Zagaris. Projecting to a slow manifold: Singularly perturbed systems and legacy codes. *SIAM Journal of Applied Dynamical Systems*, 4(3):711–732, 2005.
- [10] C. W. Gear and I. G. Kevrekidis. Constraint-defined manifolds: A legacy code approach to low-dimensional computation. *Journal of Scientific Computing*, 25(1-2):17–28, 2005.
- [11] C. W. Gear, I. G. Kevrekidis, and C. Theodoropoulos. “Coarse” integration/bifurcation analysis via microscopic simulators: micro-Galerkin methods. *Computers and Chemical Engineering*, 26:941–963, 2002.
- [12] M. Griebel, S. Knapek, G. Zumbusch, and A. Caglar. *Numerische Simulation in der Moleküldynamik: Numerik, Algorithmen, Parallelisierung, Anwendungen*. Springer, 2004.
- [13] G. Hummer and I. G. Kevrekidis. Coarse molecular dynamics of a peptide fragment: Free energy, kinetics, and long-time dynamics computations. *J. Chem. Phys.*, 118(23):10762–10773, 2003.
- [14] M. C. Jones, J. S. Marron, and S. J. Sheather. A brief survey of bandwidth selection for density estimation. *Journal of the American Statistical Association*, 91(433):401–407, 1996.
- [15] R. P. Kanwal. *Generalized Functions, Theory and Technique*. Birkhaeuser, Boston, Basel, Berlin, second edition edition, 1998.
- [16] V. Katkovnik. A new method for varying adaptive bandwidth selection. *IEEE Trans. on Signal Processing*, 47:2567–2571, 1999.
- [17] I. G. Kevrekidis, C. W. Gear, J. M. Hyman, P. G. Kevrekidis, O. Runborg, and C. Theodoropoulos. Equation-free, coarse-grained multiscale computation: Enabling microscopic simulators to perform system-level analysis. *Comm. Math. Sci.*, 1(4):715–762, 2003.
- [18] A. Lagae and P. Dutré. Poisson sphere distributions. In *Vision, Modeling, and Visualization 2006*, pages 373–379, Berlin, 2006. Akademische Verlagsgesellschaft Aka GmbH.
- [19] A. G. Makeev, D. Maroudas, and I. G. Kevrekidis. “Coarse” stability and bifurcation analysis using stochastic simulators: Kinetic Monte Carlo examples. *Journal of Chemical Physics*, 116(23):10083–10091, 2002.
- [20] H. Mori. Transport, collective motion and Brownian motion. *Prog. Theor. Physics*, 33:423–450, 1965.
- [21] W. Ren and W. E. Heterogeneous multiscale method for the modeling of complex fluids and micro-fluidics. *Journal of Chemical Physics*, 204(1):1–26, 2005.
- [22] D. W. Scott. *Multivariate Density Estimation. Theory, Practice and Visualization*. Wiley, New York, 1992.

- [23] S. J. Sheather and M. C. Jones. A reliable data-based bandwidth selection method for kernel density estimation. *Journal of the Royal Statistical Society Series B (Methodological)*, 53(3):683–690, 1991.
- [24] C. I. Siettos, M. D. Graham, and I. G. Kevrekidis. Coarse Brownian dynamics for nematic liquid crystals: Bifurcation, projective integration, and control via stochastic simulation. *Journal of Chemical Physics*, 118(22):10149–10156, 2003. Can be obtained as cond-mat/0211455 at arxiv.org.
- [25] B. W. Silverman. *Density Estimation for Statistics and Data Analysis*. Chapman and Hall, London, 1986.
- [26] P. Van Leemput, K. Lust, and I. G. Kevrekidis. Coarse-grained numerical bifurcation analysis of lattice Boltzmann models. *Physica D: Nonlinear Phenomena*, 210(1–2):58–76, 2005.
- [27] P. Van Leemput, W. Vanroose, and D. Roose. Mesoscale analysis of the equation-free constrained runs initialization scheme. *SIAM Multiscale Modeling and Simulation*, 6(4):1234–1255, 2007.
- [28] C. Vandekerckhove, I. G. Kevrekidis, and D. Roose. An efficient Newton-Krylov implementation of the constrained runs scheme for initializing on a slow manifold. Submitted, 2007.
- [29] C. Vandekerckhove, P. Van Leemput, and D. Roose. Accuracy and stability of the coarse time-stepper for a lattice Boltzmann model. *Journal of Algorithms and Computational Technology*, 2(2):249–273, 2008.
- [30] T. Werder, J. H. Walther, and P. Koumoutsakos. Hybrid atomistic continuum method for the simulation of dense fluid flows. *Journal of Computational Physics*, 205:373–390, 2005.
- [31] W. L. Winston. *Operations Research: Applications and Algorithms*. Thomson Brooks/Cole, Pacific Grove, CA, US, 4 edition, 2004.
- [32] R. Zwanzig. Nonlinear generalized Langevin equations. *Journal of Statistical Physics*, 9(3):215–220, 1973.

APPENDIX

A Kernel density estimation

We compute a kernel density estimation of the particle density for the coarse steady state, which is obtained via time integration starting from symmetric initial conditions as in Section 2.2. We consider the system to be in steady state at $t = \tau$. To assess the influence of the number of particles that is used in the KDE (4), we continue simulating the system and record the particle positions at $t = T + k\Delta\tau$, $k = 0, \dots, m - 1$, after which we use the resulting $m \cdot N$ positions in one single KDE. The results are shown in Fig. 17 (left). It can be seen that the estimate indeed converges for increasing m ; the effect of taking m small is

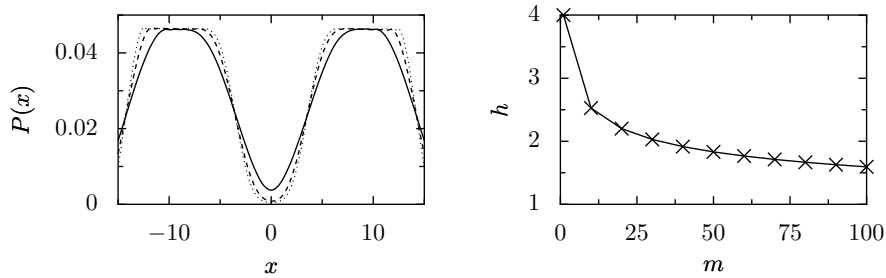


Figure 17: Left: KDE of the particle density for increasing values of m . Shown are estimates for $m = 1$ (solid), $m = 10$ (dashed) and $m = 50$ (dotted) samples. Right: Optimal bandwidth for the KDE as a function of m .

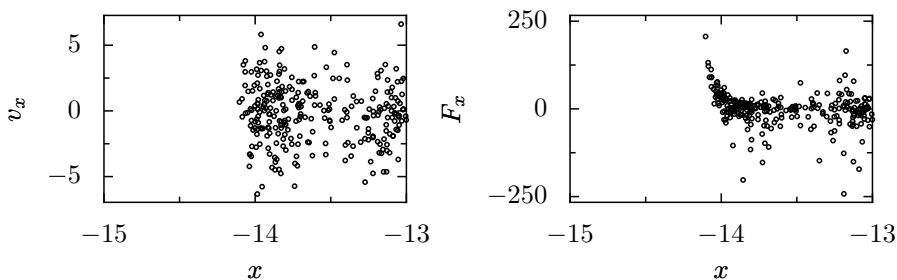


Figure 18: Typical scatter plot for particle velocities $v_{x,i}$ (left) and forces $F_{x,i}$ (right) near the left cylinder wall. Plotted is the configuration in steady state at $t = \tau = 300\,000$.

that step gradients in the density are smoothed. That this is due to the bandwidth h can be seen from Fig. 17 (right), which shows the optimal bandwidth as a function of m .

B Velocity and force

For a restart from steady state dynamics, the behavior of the system after reinitialization is analyzed more closely by considering microscopic information. We investigate individual velocity, force and positional information near the walls by looking at their x -component in a scatter plot. The result for $t = 300\,000$ of the reference run is shown in Fig. 18. The velocities (left) show a uniform particle spread, whereas the force (right) clearly marks the shape of the LJ-potential near the wall.

Equivalently, Fig. 19 shows the same picture for the restarted simulation. Comparison to Fig. 18 reveals that, at first, the particles move away from their artificial grid positions to recover a physically correct configuration. This healing process takes place over 500 MD steps.

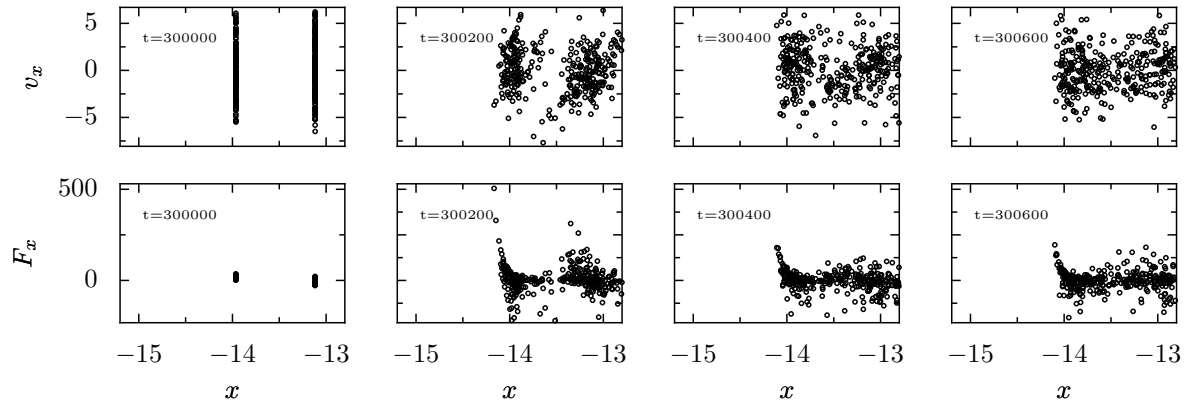


Figure 19: Evolution of the microscopic system in the $xv_{x,i}$ -plane (first row) and the $xF_{x,i}$ -plane (second row) near the left cylinder wall after reinitialization from steady state.